RESEARCH ARTICLE | OCTOBER 25 2021

Charge transport characterization of the alternative low power hybrid ion engine (*alphie*) with particle-in-cell simulations

D. Dyubo ; J. Gonzalez ; O. Tsybin ; L. Conde

Phys. Plasmas 28, 103509 (2021)
https://doi.org/10.1063/5.0060260

Physics of Plasmas ARTICLE scitation.org/journal/php

Charge transport characterization of the alternative low power hybrid ion engine (*alphie*) with particle-in-cell simulations

Cite as: Phys. Plasmas **28**, 103509 (2021); doi: 10.1063/5.0060260
Submitted: 16 June 2021 · Accepted: 1 October 2021 ·
Published Online: 25 October 2021

D. Dyubo,[1] J. Gonzalez,[2] O. Tsybin,[1] and L. Conde[3,a)]

AFFILIATIONS

[1]Institute for Physics, Nanotechnology and Telecommunications. Peter the Great St. Petersburg Polytechnic University. Polytechnichkaya 29, 195221 St. Petersburg, Russia

[2]DIFFER-Dutch Institute for Fundamental Energy Research. De Zaale 20, 5612 AJ Eindhoven, The Netherlands

[3]Departamento de Física Aplicada. E.T.S.I. Aeronáutica y del Espacio. Universidad Politécnica de Madrid. Cardenal Cisneros 3, 28040 Madrid, Spain

[a)]**Author to whom correspondence should be addressed:** luis.conde@upm.es

ABSTRACT

The Alternative Low Power Ion Engine (*alphie*) is a high specific impulse plasma thruster where both electrons and ions flow combined through the open spaces of its two-grids system. Ionizing electrons from its external cathode travel in toward the ionization chamber accelerated by the potential drop established between the grids, whereas ions exit toward the opposite direction and are later neutralized by electrons emitted from the cathode. In this configuration, the ion current is not space-charge limited, contrary to conventional gridded ion engines where only ions are transported through the grids. Since previous approaches that consider only one charged species are not valid for the *alphie* two-grids system, the characterization of geometrical parameters is studied using a fully particle-in-cell simulation. This numerical scheme calculates the velocities and positions of electrons and ions within a structured axial-symmetric mesh, which mimics one hole of the grids. The charged particle densities, currents, and their axial and radial mean velocities along the simulation domain are evaluated. Additionally, important reductions in the computational time have been obtained using different time scales for ions and electrons. Numerical results show that moderate changes in the thickness and separation of the grids with respect to the values employed in the prototype currently tested in the laboratory do not significantly affect the exhaust ion current or the ion beam collimation. Since the average velocity of the axial ions is essentially insensitive to small modifications of the geometric parameters, so will the specific impulse and thrust delivered.

I. INTRODUCTION

Electrostatic plasma thrusters (EPTs) for in-space propulsion exhaust a high velocity ion current to generate impulse. A jet of electrons and ions, usually denominated *plasma plume*, is produced when electrons are added to the ion beam to neutralize the space-charge effects.[1–3]

Plasma thrusters convert electric power into kinetic energy of ions that are accelerated to $v_{ex} \sim$ 10–40 km/s range exhaust velocities, one order of magnitude higher than those achieved by propellants in conventional chemical thrusters. This gives high specific impulses $I_{sp} = v_{ex}/g_o$, where g_o is the standard Earth's gravity. However, ion mass production rates $\dot{m}_i$ are low, and delivered thrusts $F = \dot{m}_i\, v_{ex}$ are then limited. Electrostatic plasma thrusters are, therefore, characterized by high specific impulses and low thrusts.[1–3]

Most plasma thrusters require electron sources, such as hollow cathodes for both ionization of the propellant gas and ion beam neutralization. Hall effect thrusters (HETs) and the different multi-cusp field thrusters (MCFTs) accelerate heavy ions in the self-consistent electric field created in a plasma discharge inside annular or cylindrical ionization chambers where ionizing electrons are confined by different magnetic field configurations. The physical processes involved in positive charge acceleration and propellant gas ionization are closely related in HET and MCFT thrusters.[1–3]

Gridded ion engines (GIEs) produce the electrostatic acceleration of ions extracted from a plasma source and require two electron sources. A first hollow cathode is located inside the ionization chamber to produce the ionization of the propellant neutral gas by electrons. The

ions are extracted and accelerated using a system of two or three electrically biased multi-aperture grids (plane or dish-shaped) denominated as the ion optics.[1–3]

The first *screen grid* is in contact with the plasma inside the ionization chamber; it extracts the ions and repels the electrons back. Extracted positive charges are accelerated by the electric field established between this first *screen* and the second *acceleration* grid to produce the main part of the thrust. Finally, the ion beam is neutralized by electrons from a second hollow cathode arranged in front of the ion optics.

An additional third grid biased at a low negative potential is usually located in front of the acceleration mesh to avoid the backflow of electrons from the neutralizer cathode. This additional mesh shields the acceleration grid from ion bombardment of charge-exchange ions and potentially has a longer lifetime and reduced sputtering compared with that of two-grid systems.[1,4]

The inter-grid spacing in GIEs is small (typically 1 mm) to produce high electric fields that increase the velocity of ions. These small distances combined with high voltages can cause electrical breakdown and shorting. Therefore, this sensitivity to small geometrical changes of ion optics system is an issue.

Contrary to HET and MCFT concepts, the ion production and its acceleration are independent processes in GIEs since only positive charged particles move through the grids. Thus, the maximum ion current density transported through is bounded by space-charge effects.[1,4]

The Alternative Low Power Ion Engine (*alphie*) is a new gridded plasma thruster recently introduced in Refs. 5–9. It is aimed to provide mid-sized satellites of 100–300 kg in low Earth orbit high specific impulses with thrusts within the 0.1–10 mN range at reduced power consumption (<300 W) and low propellant mass fluxes (<1 sccm) of Argon and Xenon. The measured average ion exhaust speeds 37–44 km/s of Argon ions give typical specific impulses $I_{sp} = v_{ex}/g_o$ within the 3500–4400 s range, higher than low power Hall effect thrusters.[8]

Its two-grids system operates differently from the usual GIE scheme described above. In the *alphie*, electrons and ions flow through the open spaces of its two flat parallel grids, whereas only ions move through the usual GIE ion optic system. Charges are accelerated by the self-consistent electric field created by the currents of electrons and ions in addition to the electric potential applied to the grids. Consequently, the exit ion beam is not space-charge limited. This basic *alphie* operation scheme has been investigated in the laboratory,[7,8] and it was also confirmed by particle in cell (PIC) numerical simulations.[9]

Computer modeling of propulsive systems is essential to characterize their performance and to improve designs, as it saves time and resources.[9–12] However, numerical schemes aimed at optimizing the geometry of conventional GIE ion optics that only consider the transport of ions are not valid for this new *alphie* concept.

Alternatively, the counterflow of positive and negative charged particles has been previously studied using PIC codes that generally require significant computational resources.[12–17] Specifically, characterization studies of the *alphie* two-grids system require improved codes to reduce the time consumed in calculations within affordable limits, while holding the number of simulation particles high enough to obtain realistic conclusions.

In the following, we discuss the geometrical characterization of the *alphie* two-grids system using a particle-in-cell (PIC) numerical scheme. The simulations reproduce the transport in the self-consistent electric field of charged particles through a hole of the grids using a structured axial-symmetric mesh. The particle properties such as charge and velocity are weighted in the mesh nodes, and later are used to evaluate the local self-consistent electric field. As we shall see, no significant changes in the exit ion current or in the collimation of the beam due to small changes in the geometric parameters of grids are produced.

This paper is organized as follows. The *alphie* plasma thruster conception is briefly discussed in Sec. II. The details of the PIC numerical scheme employed to study the electron and ion counterflow between the electrically biased grids and the computational domain is introduced in Secs. III and IV. The performance for a range of geometrical parameters of the two-grid systems is discussed in Sec. V, and finally, we end with some concluding remarks.

II. THE *alphie* PLASMA THRUSTER

The schematic cross section of *alphie* thuster and its electrical connections is shown in Fig. 1, and details of its operation and performance in laboratory tests can be found in Refs. 5–9.

Briefly, the cathode arranged in front of the grids provides electrons for both ionization and ion beam neutralization, similarly to HET and MCFT configurations. The Argon ions exit downstream through the flat *extraction* and *cover* grids, which are electrically biased. Typically, the extraction grid potential is $V_{EG} \simeq -150$V, and the cover grid potential V_{CG} is usually null to maximize the ion output current.[7]

A fraction of electrons from the cathode move inward through the open spaces of the grids. Inside the plasma or ionization chamber, these electrons have energies in the range of 400–500 eV energized by the $V_{AC} = 400 - 750$ V acceleration potential and are confined by the magnetic field lines (dashed lines in Fig. 1). This high energy electron group ionizes the neutral gas introduced in the plasma chamber.

Positive ions are attracted toward the extraction grid and move outward accelerated by the self-consistent electric field. They reach final exit velocities in the 40–50 km/s range controlled also by the V_{AC} acceleration voltage.[7,8] In the stationary state, this ion current is not

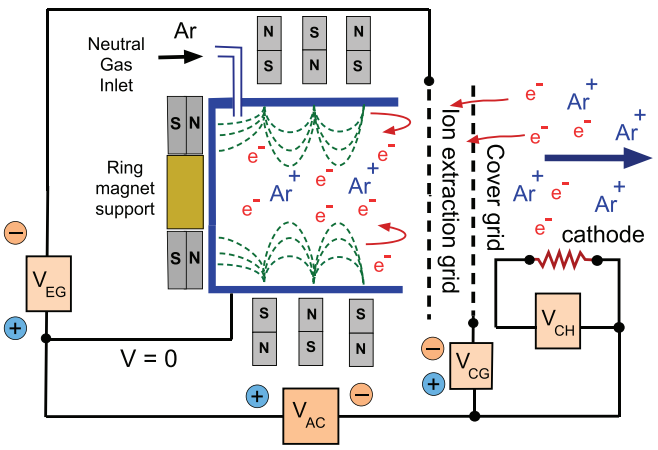

FIG. 1. Diagram of the *alphie* plasma thruster cross section and its electrical connections with Argon as propellant gas. The dotted curves represent the magnetic field lines.

space-charge limited since both positive and negative charges move through the *alphie* two-grid system. Finally, the positive charge outflow is neutralized by electrons from the cathode placed in front of the grids to form a quasi-neutral plasma plume.

Therefore, the *alphie* thruster can be categorized as a *hybrid* concept as the two grids focus and accelerate the electric charges similarly to gridded ion engines; however, it only needs one external cathode, as with HET and MCFT plasma thrusters.

III. THE NUMERICAL SIMULATION DOMAIN

The grids in the *alphie* prototype currently tested in the laboratory are two stainless steel disks with 665 aligned holes of 1 mm in diameter drilled within a circle of 20 mm in radius. Figure 2 represents schematically the axial-symmetric simulation domain of two aligned holes where t_G is its thickness and d_G their separation. In our numerical simulations, the position of the first extraction grid is fixed at $d_E = 2.0$ mm of the upstream boundary at $z_U = 0.0$ mm, and the ion downstream exit section z_D is located at the $d_C = 5.0$mm distance from the cover grid. The end of the cover grid is located at $z_E = d_E + d_G + 2\,t_G$, as shown in Fig. 2. The metallic ionization chamber of Fig. 1 is considered at zero voltage ($V = 0$), and it is also the reference for the electric potentials applied to the grids.

In the current prototype $d_G = 2.0$ mm, $t_G = 0.5$ mm and these values will be used in the following as a reference. These geometrical parameters will be modified in the following to study their impact in the electron and ion currents transported through the two-grids system.

As shown in Fig. 2, the *upstream* region $z < d_E$ represents the ionization chamber of the scheme in Fig. 1, whereas the *downstream* side is the vacuum in front of the cover grid. The grids are typically biased to -150 and -600 V with respect to the upstream boundary kept at 0V. Typical thruster currents in the experiments are $I_E \simeq 100$–500 mA that giving 150–750 μA transported through the computational domain of Fig. 2.

The boundary conditions are similar to those of Ref. 9. The electric potential at z_U is assumed as null to match the ionization chamber potential, and the axial electric field is zero at the opposite side z_D, in the distant quasineutral plasma. At the maximum radial position and along the axis of symmetry, radial component of the electric field is considered as null.[9]

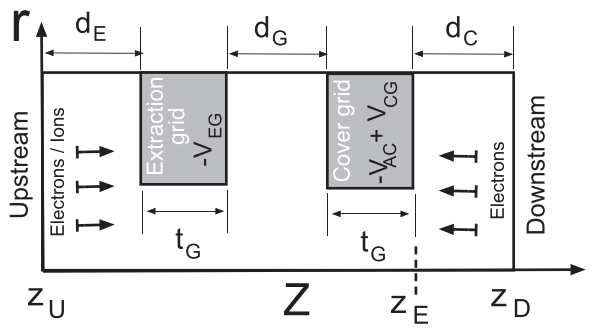

FIG. 2. The axial-symmetric simulation domain of two aligned holes. The ionization chamber electrically biased at zero potential is located upstream at $z < z_U$, and the cathode is located at the $z > z_D$ downstream side. The coordinate z_E indicates the exit section of the cover grid.

Electrons from the cathode enter the downstream side $z = z_D$ of the computational domain and ions and electrons enter from the upstream ionization chamber. Two populations of electrons coexist in the $z < d_E$ region confined by the negative potential of the extraction grid and the magnetic field lines. The fast electrons from the cathode and the slow group resulting from the impact ionization of neutral atoms upstream. Only electrons from the cathode and exiting ions are present on the downstream side.

The initial electron and ion temperatures, densities, and velocities in the simulation domain were selected to match typical plasma conditions. Electrons from the cathode are introduced at the downstream side with a temperature of 2500 K and axial mean velocity of -87 km/s. Secondary electrons from ionization processes at the plasma chamber have also an axial velocity of 87 km/s and a temperature of 500 K. The ions enter upstream in the simulation region with a mean velocity of 300 m/s and a temperature of 500 K. The typical reference density for both species is on the order of 10^{15} m^{-3}, giving a Debye length of 0.1 mm. From the downstream side of the mesh, a current of 150 μA of electrons is injected, and at the ionization chamber, side currents for ions and electrons are one order of magnitude below. Finally, when a charged particle exits the numerical domain or collides with the grids, it is removed from the simulation.

IV. THE *fpakc* PIC NUMERICAL SCHEME

The usual simulation scheme where electrons are in thermal equilibrium following a Boltzmann energy distribution and ions are treated as particles is not valid to describe the charged particle counterflow through the *alphie*'s two-grids system. A full particle-in-cell code where both ions and electrons are considered as macro-particles driven by the local electric field is required to study the charge transport through the simulation domain of Fig. 2.

The numerical scheme employed in our calculations, now named Finite element PArticle Kinetic Code (*fpakc*), is an evolution of a previous particle-in-cell code discussed in Ref. 9. The current version can tackle different problems by means of an input file, and the previous original uniform finite difference grid has been replaced by a finite element mesh. Additionally, the possibility of advancing the different particle species with specific time scales has been also introduced. These two new capabilities are of major importance for the grid characterization analysis of *alphie* thruster concept. The predictions of previous codes[9] and *fpakc* were validated against the experimental data of Ref. 7.

The finite element mesh allows adapting the simulation domain to different geometries; however, a structured mesh is still preferred for the present case. The axial-symmetric computational domain of Fig. 2 is divided in a structured rectangular mesh of cells of about 0.1 mm side length.

As with most PIC codes, the *fpakc* numerical scheme runs for a number of iterations until a quasi-steady state is reached. At each iteration, new particles are injected into the simulation domain of Fig. 2 at both boundaries. All the particles, old and new, are pushed to obtain their new coordinates and velocities. They can move to a different cell or interact with those at adjacent cells, tracked in *fpakc* by means of a neighbor interaction system. Cells and material surfaces are linked by the nodes they share, reducing the computational cost of assigning particles to specific cells in the simulation. About 10^6 macro-particles are present in the domain when a quasi-steady state is reached. Then,

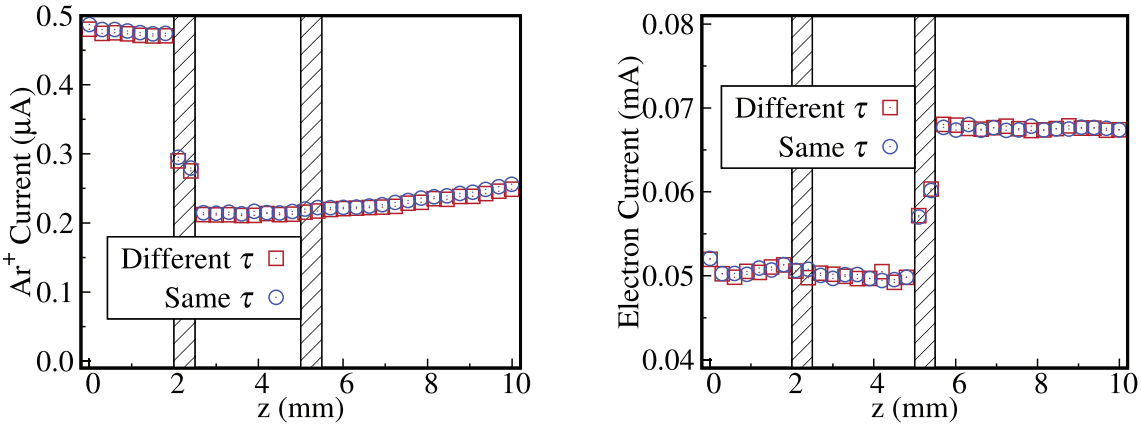

FIG. 3. Comparison of electron and ion currents flowing through the simulation domain of Fig. 2 calculated with equal iteration time $\tau = 10^{-11}$ s (open circles) and when it is increased to $\tau = 10^{-9}$ s for the ions (open squares).

the properties of the particles (essentially charge and velocity) are deposited in the nodes of the cells in which the particles end their motion after each iteration. The self-consistent electric field is computed locally in the finite element mesh by solving the Poisson equation.

The ability to push species with different time scales is essential to reduce computational time. This is a critical issue in situations where both, ions and electrons, are included in the simulation as mobile kinetic species. In the present case, light electrons from the cathode move much faster through the *alphie* two-grids system than the slow and heavy ions. The multiple timescale feature of the *fpakc* numerical scheme is illustrated in Figs. 3 and 4.

Figure 3 shows the position of the two grids, which is indicated by the dashed areas and also the values of the electron $I_e(z)$ and ion $I_i(z)$ currents flowing along the computational domain of Fig. 2. Both are evaluated as averages over the velocity distribution function of particles along the cells of the simulation domain.

The current I_z is calculated from the axial current density $J_z = n\,v_z$ obtained in the structured grid nodes. The integration is approximated by

$$I_z = \int_0^{r_{max}} 2\pi\, r\, J_z(r) dr \simeq \sum_{j=0}^{5} 2\pi \frac{r_j + r_{j+1}}{2} \frac{J_{z,j} + J_{z,j+1}}{2} (r_{j+1} - r_j),$$

where j represents the node along the radial direction.

The calculated Argon ion current per hole remains in Fig. 3(a) approximately equal for $z < 2.2$ mm inside the ionization chamber. After the extraction grid, $I_i(z)$ decreases due to the unavoidable losses by the capture of ions on its surface. The ion current remains constant as positive charges gain positive velocity outward and exit the cover grid. Due to the self-consistent radial field outside the grid system, ions become even more collimated, resulting in a slight increase in current as axial velocity increases. Since the holes of both meshes are aligned, ion losses are much lower in the second grid. Due to the self-

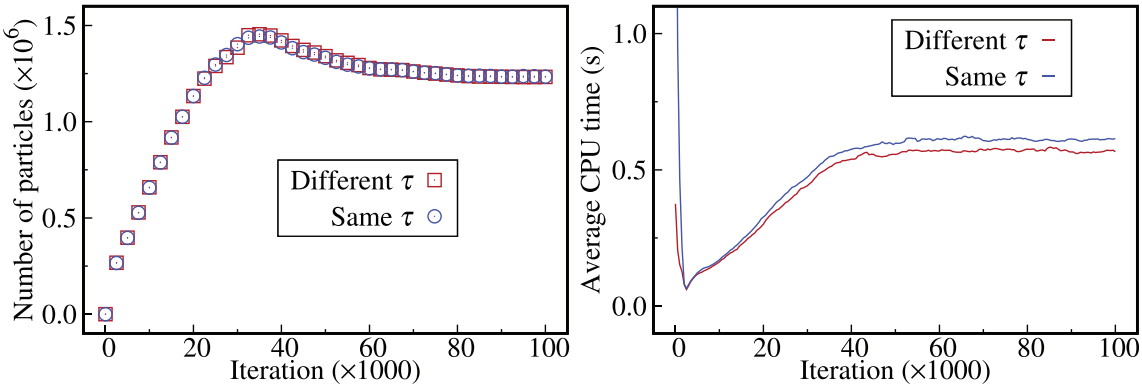

FIG. 4. Comparison of numerical simulation performance using equal time step of $\tau = 10^{-11}$ s for ions and electrons (dotted lines) and when it is increased to $\tau = 10^{-9}$ s for the ions (solid lines).

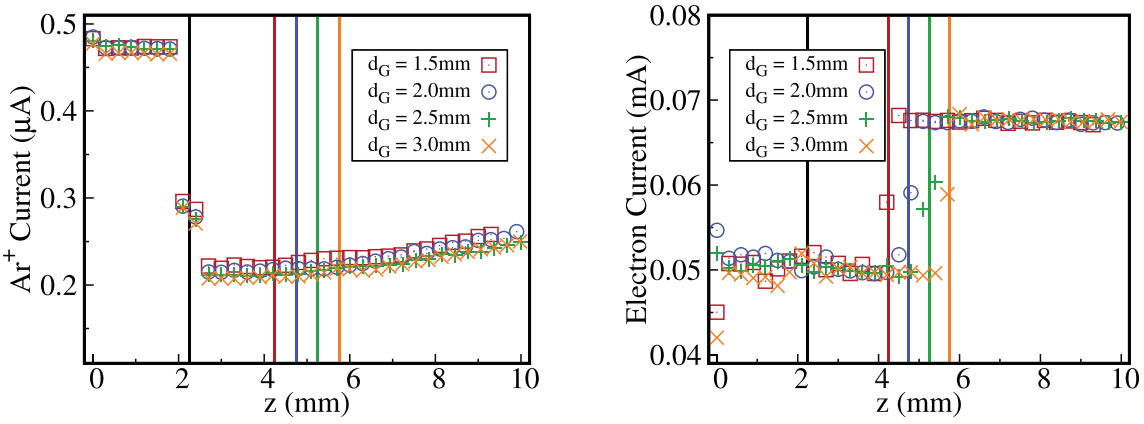

FIG. 5. The ion and electron current for different distances d_G between the extraction and cover grids. The grid thickness remains constant to the base case of $t_G = 0.5$ mm. Vertical lines represent the mid position of grids.

consistent electric field created by the counterflow of charges and the boundary conditions set at the end of the numerical domain, a slight increment in the current appears. However, present study concerns the changes in the ion distribution at the exit plane $z_E < z_D$ of the two-grids system in Fig. 2.

The electron current in Fig. 3(b) follows the opposite trend. Its value is approximately constant for $z > 6$ mm in the region in front of the cover grid where the cathode is located. Electrons are absorbed by the cover grid and lost in the simulation, and consequently, the electron current reduces to remain essentially constant in the inter-grid space and for $z < 2$ mm. Thus, the electron current becomes more negative in the inter-grids space since electrons are accelerated inward and finally takes its minimum value within the ionization chamber because of the high velocity of ionizing electrons. The difference in magnitude of the electron and ion currents in Fig. 3 is caused by the high negative velocity of electrons, much higher than the average ion speed.

Figure 3 shows that numerical results obtained for the $I_e(z)$ and ion $I_i(z)$ currents are equal using the equal $\tau = 10^{-11}$s timescale for iteration (open circles) and when it is increased to $\tau = 10^{-9}$s for the ions. The number of macro-particles present in the simulation Fig. 4(a) is essentially the same as ions and electrons iterate with the same time step of (open squares) or when this timescale is increased for ions by a factor 100. In this last case, the effort required for these calculations in Fig. 4(b) shows a reduction of 40% in the total computational time.

V. NUMERICAL RESULTS

We study in first place the effect of the distance d_G between the extraction and cover grids, holding constant their thickness t_G. As it was in Fig. 3, the currents $I_i(z)$ of ions moving upstream and electrons $I_e(z)$ flowing inward to the ionization chamber are represented in Fig. 5 along the axial direction of symmetry.

The solid vertical lines indicate the midpoint position of the two *alphie* grids for the distances $d_G = 1.5$, 2.0, 2.5, and 3.0 mm for a constant grid thickness of $t_G = 0.5$ mm. The location of the extraction grid was held fixed and the cover grid displaced along the axis of symmetry of the simulation domain.

The changes with the distance d_G in the electron and ion currents in Fig. 5 are minimal. Reductions in the distance between the grids only produce small increments in the ion current $I_i = I_{i,z}(z_E)$ at the exit section of the cover grid of Fig. 5(a). We have observed no differences between 2.5 and 2.0 mm separation distances. The effect in the electron current $I_e(z)$ is even smaller as it can be observed in Fig. 5(b). The self-consistent electric field generated between the grids by the counterflow of charges explains why reductions in the distance between the two grids have small effect in the magnitude of the ion and electron currents.

Figure 6 represents the ion density radial profile $n_i(r, z_E)$ at the z_E coordinate, corresponding to the exit plane of the cover grid for $d_G = 1.5$, 2.0, 2.5, and 3.0 mm. Its value is maximum at the axis of symmetry $r = 0$ and decreases faster with the radial distance r for shorter separations between the grids. Since the ion current $I_i(z)$ in Fig. 5(a) is essentially independent of the separation between grids, the

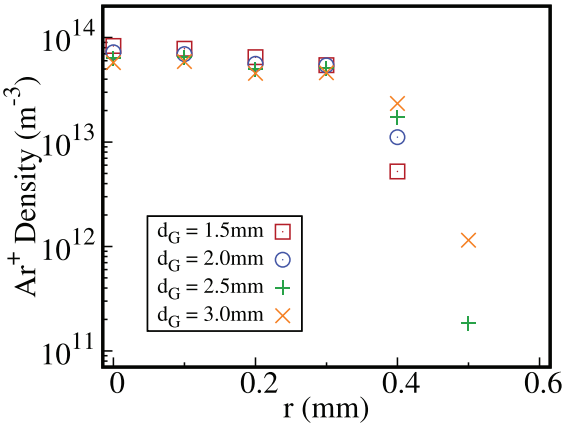

FIG. 6. The axial number density $n_i(r, z_E)$ of ions for different distances d_G between the extraction and cover grids, holding constant $t_G = 0.5$ mm.

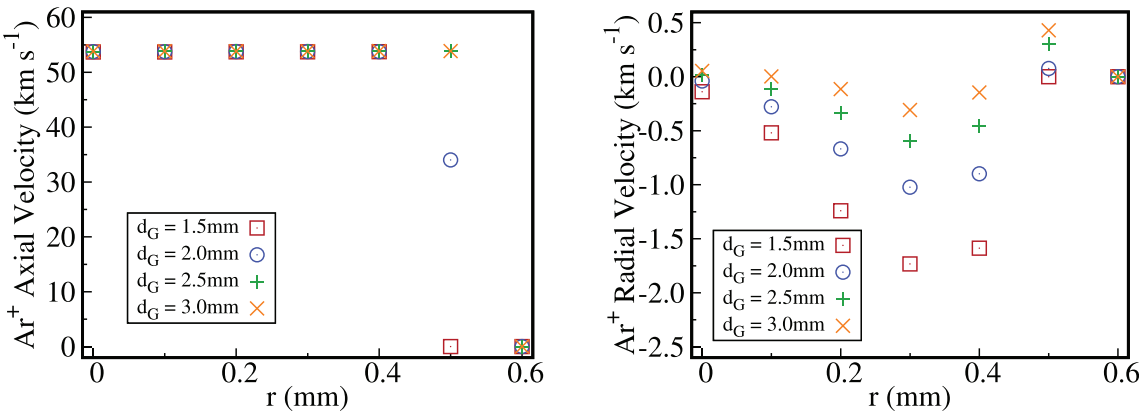

FIG. 7. The axial ion $v_{i,z}(r, z_E)$ and radial $v_{i,r}(r, z_E)$ velocities for different distances d_G between the extraction and cover grids of Fig. 2, holding constant $t_G = 0.5$ mm. Non-zero radial velocity at the axis comes from the weighting of particles into the axis nodes.

exit ion beam becomes more focused as the distance d_G reduces. Therefore, ions concentrate along the hole centerline when the distance between grids is reduced.

This ion collimation effect as d_G decreases is also observed in Fig. 7 that shows the average axial $v_{i,z}(r, z_E)$ and radial $v_{i,r}(r, z_E)$ components of the ion velocity at the exit plane.

The axial velocity of ions in Fig. 7(a), within the 10–55 km/s range, is in accordance with those measured in the laboratory.[7] They decrease faster with r for smaller distances d_G between the grids. The radial component in Fig. 7(b) is 1–2 orders of magnitude lower than $v_{i,z}(r, z_E)$ and remains negative for most cases, except for $d_G \geq 2.5$ mm. The non-zero radial velocity at the axis comes from the weighting of particles into the finite element mesh, as some may be far from the axis but still deposit some information into the axis nodes. This shift in radial velocity indicates that the ion beam becomes more skew.

Additionally, small changes in the thickness t_g of grids also have a low impact in the electric charge transport. Figure 8 shows the ion $I_i(z)$ and electron $I_e(z)$ currents flowing, respectively, downstream and upstream of the simulation domain for $t_G = 0.3, 0.4, 0.5$, and 0.6 mm holding constant the separation $d_G = 2.0$ mm between both meshes.

Increments in $I_i(z)$ as t_G is reduced are small, and the electron current $I_e(z)$ remains unaltered. Both have similar values to those of Fig. 5(a), and variations in the plasma density in the ionization chamber are essentially responsible for the increments in the ion current downstream the cover grid. The larger reduction observed for $t_G =$ 0.6 mm seems to be related to the increased particle losses for thick grids.

The radial profile of ion density $n_i(r, z_E)$ at the exit plane of the cover grid in Fig. 9 is insensitive to changes in the thickness of both grids. This is also the case for the axial and radial components of the

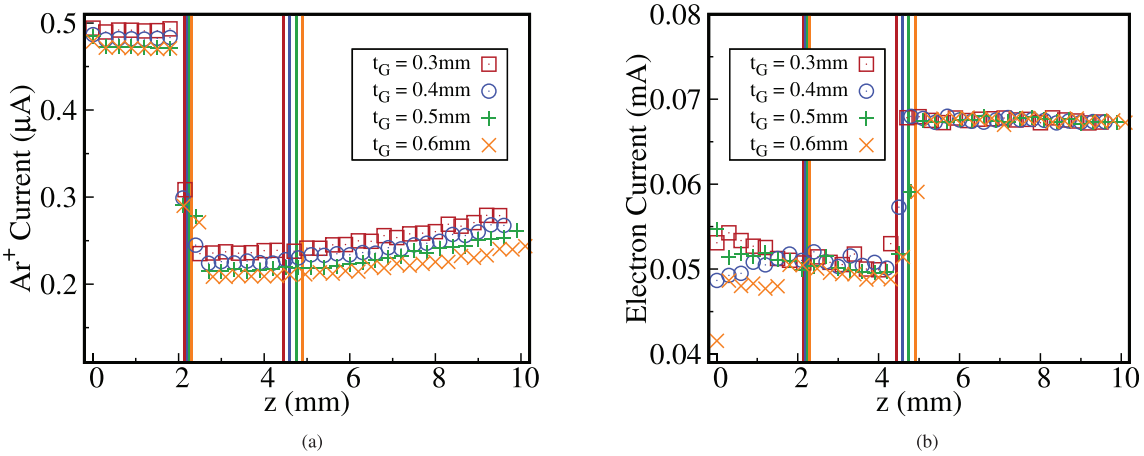

FIG. 8. The currents of ions and electrons for different grid thicknesses t_G of the extraction and cover grids of Fig. 2. The separation between grids remains constant to the base case of $d_G = 2.0$ mm. Vertical lines represent the mid position of grids for each case.

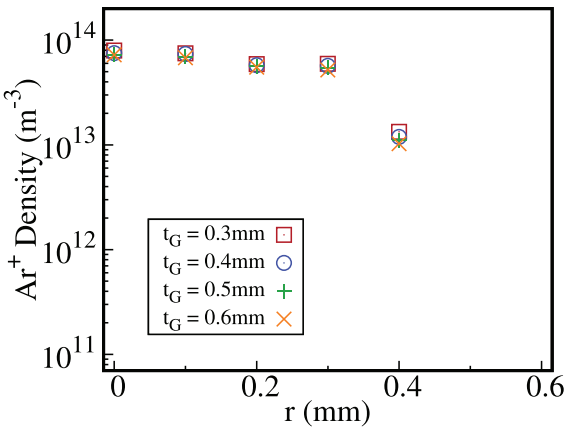

FIG. 9. The axial number density $n_i(r, z_E)$ of ions along the radial direction of Fig. 2 for different grid thicknesses t_G of the extraction and cover grids, holding constant $d_G = 2.0$ mm.

average ion velocity in Fig. 10. Thus, the ones and electron dynamics seem unaltered by grid thickness.

VI. CONCLUSIONS

The characterization of the *alphie* two-grids system requires a different numerical approach than those used for ion optics of conventional GIEs. In this last case, only ions travel through the open spaces of the grids, whereas a counterflow of ions and electrons is transported through an *alphie* thruster. The ion current is not space-charge limited since the local electric field is self-consistently determined by the electric potential applied to the grids and the ion and electron flows.

This electric charge transport has been simulated using the *fpakc* particle-in-cell code where different time scales can be used for the ion and electron time evolutions. This feature reduces about 40% of the computational time and permits exploration of changes in the basic geometry of the *alphie* two-grids system.

Both ions and electrons are simulated from a kinetic point of view, necessary to describe the influx of high energy electrons, that is a unique characteristic of *alphie* thruster operation. Moreover, the code calculates the velocities and positions of both species of particles, allowing a detailed analysis of the performance impact of geometrical parameters.

The counterflow of positive and negative charges produces a focused ion flow along the axis of symmetry as shown by the large difference between the axial and radial components of the ion velocity in Figs. 7 and 10. The ions are concentrated along the centerline of the simulation domain, and the collimation of the beam basically depends on the distance d_G between the extraction and cover grids, as shown in Figs. 6 and 9.

However, the calculations in Figs. 5 and 8 indicate that small changes in the distance d_G between the grids and their thickness t_G have minimal impact in the ion current $I_i = I_{i,z}(z_E)$ at the exit plane of the cover grid of Fig. 2. Assuming single-charged ions for simplicity, the thrust delivered $F = \dot{m}_i v_{i,z}$, where $\dot{m}_i = m_i \times I_i/e$ also will be essentially constant for small changes in d_G and t_G.

We can conclude that the *alphie* two-grids thruster concept is robust. Small variations in the distance between the grids and their thickness have little impact in both the exhaust ion beam and the inflow of ionizing electrons from the cathode. Therefore, it is potentially insensitive to moderate modifications of its basic geometry originated by the unavoidable wear during long-term thruster operation.

The ion current and beam collimation are not significantly affected by changes in the grid thickness. Therefore, this parameter can be selected according to other considerations, such as their mechanical characteristics or thruster manufacture. In addition, the spacing between the *alphie* grids is longer than those of conventional GIEs (usually around 1 mm), which reduces the chances of sparks and electrical breakdowns between them.

The results of Figs. 7 and 10 show that the axial velocity of ions, directly related to the specific impulse and thrust, is essentially unaltered by small geometrical variations in the *alphie* two-grids system. This hints that small deformations or erosion of the grids by sputtering will have a lesser impact in the thruster performance, unlike classical GIEs. However, this issue requires of further numerical analysis and endurance laboratory tests.

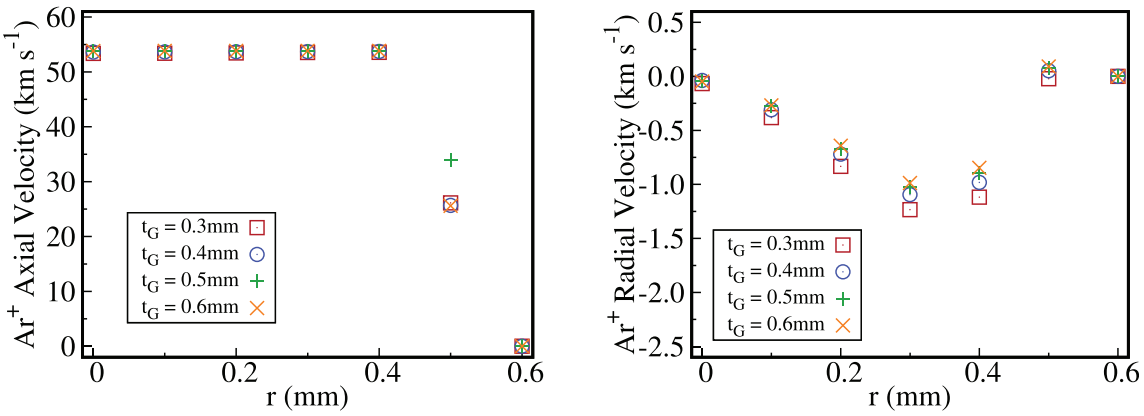

FIG. 10. The axial ion $v_{i,z}(r, z_E)$ and radial $v_{i,r}(r, z_E)$ velocities for different grid thicknesses t_G of the extraction and cover grids, holding constant $d_G = 2.0$ mm.

ACKNOWLEDGMENTS

This work was partially funded by the Ministerio de Ciencia, Innovación y Universidades of Spain under Grant No. RT2018–094409-B-100 and also by the Russian Scientific Foundation under Grant No. 21–72-20029.

DATA AVAILABILITY

The data that support the findings of this study are available from the corresponding author upon reasonable request.

REFERENCES

[1]D. M. Goebel and I. Katz, *Fundamentals of Electric Propulsion. Ion and Hall Thrusters* (John Wiley & Sons, Hoboken, NJ, 2008).
[2]S. Mazouffre, Plasma Source Sci. Technol. **25**, 033002 (2016).
[3]I. Levchenko, S. Xu, S. Mazouffre, D. Lev, D. Pedrini, D. Goebel, L. Garrigues, F. Taccogna, and K. Bazaka, Phys. Plasmas **27**, 020601 (2020).
[4]M. Sangregorio, X. K. N. Wang, N. Guo, and Z. Zhang, Chin. J. Aeronaut. **31**, 1635 (2018).
[5]L. Conde, J. L. Domenech-Garret, J. M. Donoso, E. D. Río, and M. A. Castillo, "Plasma accelerator with modulated thrust," U.S. Patent No. 10,172,227 B2 (2019).
[6]L. Conde, J. L. Domenech-Garret, J. M. Donoso, E. Del Río, and M. A. Castillo, "Plasma accelerator with modulated thrust and space born vehicle with the same," EPO Patent No. EP3369294B1 (2015).
[7]L. Conde, J. Domenech-Garret, J. Donoso, J. Damba, S. Tierno, E. Alamillo-Gamboa, and M. Castillo, Phys. Plasmas **24**, 123514 (2017).
[8]L. Conde, J. González, J. Donoso, J. Domenech-Garret, J. Damba, P. Maldonado, J. Grabulosa, and M. Lahoz, in *Proceedings of the 36th International Electric Propulsion Conference* (IEPC, Vienna, Austria, 2019), pp. 1–9.
[9]J. González and L. Conde, Phys. Plasmas **26**, 043505 (2019).
[10]D. Dyubo and O. Y. Tsybin, SPbPU J-. Phys. Math. **13**, 78 (2020).
[11]S. Cho, H. Watanabe, K. Kubota, S. Iihara, K. Fuchigami, K. Uematsu, and I. Funaki, Phys. Plasmas **22**, 103523 (2015).
[12]I. Hutchinson, Phys. Plasmas **24**, 055601 (2017).
[13]S. Hosseini Jenab and F. Spanier, Phys. Rev. E **95**, 053201 (2017).
[14]H. Kim, F. Iza, S. Yang, M. Radmilović-Radjenović, and J. Lee, J. Phys. D: Appl. Phys. **28**, R283 (2005).
[15]V. Kobolob and R. Arslanbekov, J. Phys.: Conf. Ser. **719**, 012020 (2016).
[16]D. Tskhakaya, K. Matyash, R. Schneider, and F. Taccogna, Contrib. Plasma Phys. **47**, 563 (2007).
[17]L. Liu, W. Zou, H. Wang, F. Guo, and D. Liu, Phys. Plasmas **25**, 022502 (2018).